

# Spin demons in $d$ -wave altermagnets

Pieter M. Gunnink,<sup>1,\*</sup> Jairo Sinova,<sup>1</sup> and Alexander Mook<sup>1</sup>

<sup>1</sup>*Johannes Gutenberg University Mainz, Staudingerweg 7, Mainz 55128, Germany*

(Dated: July 14, 2025)

Demons are a type of plasmons, which consist of out-of-phase oscillations of electrons in different bands. Here, we show that  $d$ -wave altermagnets, a recently discovered class of collinear magnetism, naturally realize a spin demon, which consists of out-of-phase movement of the two spin species. The spin demon lives outside of the particle-hole continuum of one of the spin species, and is therefore significantly underdamped, reaching quality factors of  $> 10$ . We show that the spin demon carries a magnetic moment, which inherits the  $d$ -wave symmetry. Finally, we consider both three and two dimensional  $d$ -wave altermagnets, and show that spin demons exists in both.

*Introduction.* Altermagnets are a recently discovered class of collinear magnets, characterized by a sublattice transposing symmetry involving rotation or mirror operations [1, 2]. Their anisotropically spin-split Fermi surfaces exhibit a  $d$ -wave (or higher even-parity) order. These spin-split bands can give rise to unusual transport properties [2–4], piezomagnetism [5, 6], the generation of spin-splitter torque in MRAM geometries [7] and chiral split magnon bands [8–10].

The existence of spin-split Fermi surfaces also opens up the possibility of an out-of-phase oscillation of the two spin densities, realizing a *demon*: an acoustic, electrically neutral type of plasmon, first proposed by Pines [11] in 1956 and only observed by Husain *et al.* [12] in 2023. Demons are gapless, in contrast to the conventional in-phase charge plasmon in three dimensions, and have been predicted for numerous materials [11, 13–16]. Importantly, demons are not infinitely long-lived quasiparticles, because they have finite overlap with the particle-hole continuum. This overlap can however be reduced with sufficient separation of the Fermi surfaces, suppressing the damping and thus forming well-defined quasiparticles with high quality factors [12, 17]. Besides being relevant as a long-lived quasiparticle, demons have also been proposed to affect phase-transitions [18], couple to phonons [19] and induce superconductivity [13, 16, 20].

In this work, we show that in a  $d$ -wave altermagnetic metal, the spin-split bands naturally host a out-of-phase oscillation of the spin densities—thus realizing a spin-polarized demon, which we dub a *spin demon*. The spin demon does not live completely outside of the particle-hole continuum, but only outside of the particle-hole continuum of one of the spin species. The spin demon is therefore not completely undamped, but can still reach quality factors of  $> 10$  for realistic parameters and is therefore well defined and long lived. We demonstrate the existence of the spin demon in both a three-dimensional (3D) and two-dimensional (2D)  $d$ -wave altermagnetic metal. We also establish that the spin demon inherits the  $d$ -wave symmetry of the altermagnetic order parameter, by demonstrating that it has a finite magnetic moment which changes sign as the demon’s propagation direction is rotated through the altermagnetic spin-split plane.

The primary signature of the spin demon is a strongly peaked response in the imaginary part of the spin-spin response function,  $\text{Im}[\chi_{S_z S_z}(\mathbf{q}, \omega)]$ , as shown in the altermag-

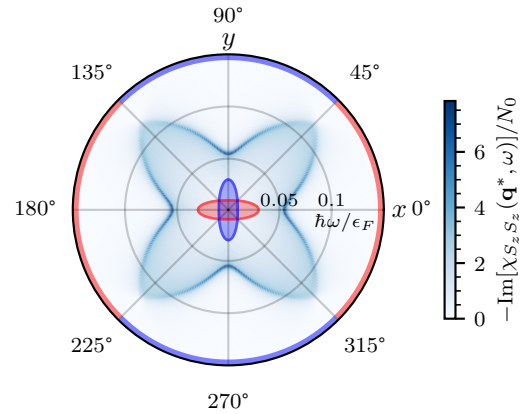


FIG. 1. The imaginary part of the spin–spin response function,  $\text{Im}[\chi_{S_z S_z}(\mathbf{q}^*, \omega)]$ , where  $\mathbf{q}^* = q (\cos \theta, \sin \theta, 0)$ , rotated in the altermagnetic spin-split plane with a fixed  $q = 0.05k_F$ . The angular direction encodes  $\theta$  and the radial axis the frequency  $\omega$ . The colors on the ring indicate the projected spin species, with red (blue) spin up (down). The spin demon is the sharp resonance that follows the four-fold rotational symmetry of the  $d$ -wave altermagnet. The anisotropically spin-split Fermi surfaces are schematically shown at the origin (not to scale).

netic spin-split plane in Fig. 1. It follows the four-fold rotational symmetry of the  $d$ -wave altermagnet, vanishing along the high-symmetry axis, where the electron bands are degenerate. In the four different quadrants of the altermagnetic spin-split plane, the majority spin species in this out-of-phase oscillation changes, following the altermagnetic  $d$ -wave symmetry.

*Method.* We describe the spin demon within the random phase approximation (RPA), where the spin-resolved response functions  $\chi_{\sigma\sigma'}$  follow [21]

$$\begin{pmatrix} \chi_{\uparrow\uparrow} & \chi_{\uparrow\downarrow} \\ \chi_{\downarrow\uparrow} & \chi_{\downarrow\downarrow} \end{pmatrix}^{-1} = \begin{pmatrix} \chi_{\uparrow}^{(0)} & 0 \\ 0 & \chi_{\downarrow}^{(0)} \end{pmatrix}^{-1} - v_q \begin{pmatrix} 1 & 1 \\ 1 & 1 \end{pmatrix}. \quad (1)$$

Here,  $\chi_{\sigma}^{(0)}$  is the non-interacting density-density response function for spin  $\sigma$  and  $v_q = e^2/\epsilon_0 q^2$  is the Fourier transform of the Coulomb interaction, with  $q = |\mathbf{q}|$ . We assume the altermagnet to be oriented such that the spin-splitting is maximal along the  $x, y$ -axis. The low-energy dispersion of a (planar)

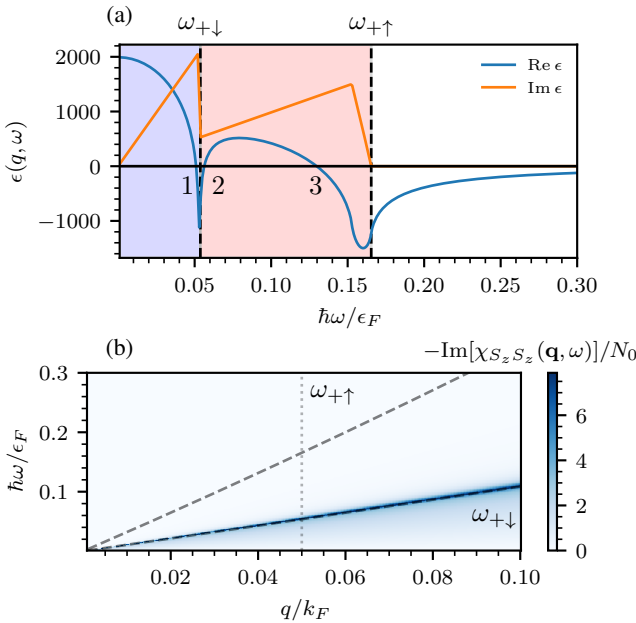


FIG. 2. (a) The real and imaginary part of the dielectric function, for  $\mathbf{q}^* = q\hat{\mathbf{x}}$ , with  $q = 0.05k_F$ . The zeros of the real part correspond to resonances, the imaginary part determines their damping. The spin demon is the second zero. The blue and red shading indicate where the spin-down and spin-up particle-hole continua is non-zero. (b) The imaginary part of the spin-spin response function,  $\text{Im}[\chi_{S_z S_z}(\mathbf{q}, \omega)]$ , for  $\mathbf{q} = q\hat{\mathbf{x}}$ , showing the existence of a spin demon with a high quality factor. The vertical dotted line corresponds to the  $q$  used in (a). In both (a,b), the dashed lines indicate the spin-resolved particle-hole continua edges,  $\omega_{+\sigma}$ .

*d*-wave altermagnet is described by [2]

$$\epsilon_{\mathbf{k}}^{\sigma} = \frac{\hbar^2 k^2}{2m_0} + \sigma \frac{\hbar^2 (k_x^2 - k_y^2)}{2m_*}, \quad (2)$$

where we take  $m_0 = 0.4m_e$ ,  $m_* = 1.25m_0$  and a Fermi level of  $\epsilon_F = 0.5$  eV. Here,  $m_e$  is the electron mass. The non-interacting density-density response function can be found analytically from the Lindhard function [22]; we show details in Secs. I and II in the Supplemental Material (SM) [23]. Solving Eq. (1) for  $\chi_{\sigma\sigma}(\mathbf{q}, \omega)$ , we find the three response functions  $\chi_{nn}(\mathbf{q}, \omega)$ ,  $\chi_{nS_z}(\mathbf{q}, \omega)$ ,  $\chi_{S_z S_z}(\mathbf{q}, \omega)$  [21]. We focus on  $\chi_{S_z S_z}(\mathbf{q}, \omega)$ , which shows the strongest signature of the spin demon:

$$\chi_{S_z S_z}(\mathbf{q}, \omega) = \frac{\chi_{\uparrow}^{(0)} + \chi_{\downarrow}^{(0)} - 4v_q \chi_{\uparrow}^{(0)} \chi_{\downarrow}^{(0)}}{\epsilon(\mathbf{q}, \omega)} \quad (3)$$

where

$$\epsilon(\mathbf{q}, \omega) \equiv 1 - v_q (\chi_{\uparrow}^{(0)} + \chi_{\downarrow}^{(0)}) \quad (4)$$

is the complex longitudinal dielectric function. We discuss  $\chi_{nn}(\mathbf{q}, \omega)$  and  $\chi_{nS_z}(\mathbf{q}, \omega)$  in Sec. III in the SM [23].

Collective modes emerge as the poles of the response function, determined by the zeros of the longitudinal dielectric

function,

$$\epsilon(\mathbf{q}, \omega) = 0, \quad (5)$$

resulting in a peak in the imaginary part of the response function [21].

We first analyze the dielectric function in more detail, by showing  $\epsilon(\mathbf{q}, \omega)$  for a fixed  $\mathbf{q} \parallel \hat{\mathbf{x}}$  in Fig. 2(a), where we also indicate the spin-polarized particle-hole continua, which edges are given by  $\omega_{+\sigma} = v_F^{\sigma} \cdot \mathbf{q} + O(q^2/k_F^2) = \eta_{\sigma}(\theta)v_F q + O(q^2/k_F^2)$ , where  $\eta_{\sigma}(\theta)$  and  $v_F$  are defined in Eq. (6).

We observe the existence of three zeros of the dielectric function. The first and third zero correspond to the spin-down and spin-up acoustic plasmon respectively [24, 25], which are overdamped because they live in their respective particle-hole continuum. The second zero however arises because of the interplay of the spin-up and spin-down particles, and we claim here that this corresponds to a spin demon. We show the evolution of the three zeros of the dielectric function in the altermagnetic spin-split plane in more detail in Sec. IV in the SM [23]. Importantly, the spin demon sits outside of the spin-down continuum, and therefore the imaginary part of the dielectric function is reduced. This implies that the spin demon is potentially underdamped.

We show the underdamped character of the spin demon in more detail with the imaginary part of the spin-spin response function,  $\text{Im}[\chi_{S_z S_z}(\mathbf{q}, \omega)]$  in Fig. 2(b). As noted earlier, collective modes result in peaks in the imaginary part of a response function, with the width of the peak inversely proportional to its lifetime. We observe in Fig. 2(b) a sharply peaked resonance close to the edge of the spin-down continuum—which we identify as the spin demon from our previous analysis of the zeros of  $\epsilon(\mathbf{q}, \omega)$ . We stress that the spin demon is not completely undamped, due to a finite overlap with the spin-up continuum.

We show in Sec. V in the SM [23] the imaginary part of the spin-spin response function  $\text{Im}[\chi_{S_z S_z}(\mathbf{q}, \omega)]$  for a larger range of  $q$  values, from which we conclude that for this set of parameters, the spin demon remains well defined for  $q/k_F \lesssim 0.5$ .

Upon rotation through the altermagnetic spin-split plane, we obtain Fig. 1, demonstrating that the spin demon is most sharply defined along  $x$  and  $y$ , and vanishes along the nodal lines, where the Fermi surfaces are spin degenerate. The spin demon remains well defined for small tilt angles off the altermagnetic spin-split plane, as shown in Sec. VI in the SM [23].

*Analysis.* In what follows, we constrain  $\mathbf{q}$  to lie in the altermagnetic spin-split plane, parametrizing  $\mathbf{q} = q(\cos \theta, \sin \theta, 0)$ . Our analysis is simplified by defining the projected spin splitting of the particle-hole continuum for spin species  $\sigma$ :

$$\eta_{\sigma}(\theta) \equiv \sqrt{\tilde{m} m_0 \left(1 + \sigma \frac{m_0}{m_*} \cos 2\theta\right)}, \quad (6)$$

where  $\tilde{m} \equiv m_0(m_*^2/(m_*^2 - m_0^2))^{1/3}$ . We have defined  $\eta_{\sigma}(\theta)$  such that  $\chi_{\sigma}^{(0)}$  can be obtained from the well-known Lindhard

function for spherical Fermi surfaces [21, 26] by rescaling  $q \rightarrow \eta_\sigma(\theta)q$  and  $m \rightarrow \tilde{m}$  [22]. For convenience, we define a spin-independent Fermi wave vector  $k_F \equiv \sqrt{2\tilde{m}E_F}/\hbar$  and velocity  $v_F \equiv \hbar k_F/\tilde{m}$ .

The analysis is simplified by noting that, depending on the angle  $\theta$ , one of the two spin species can be treated as the (projected) majority spin species, defined such that  $\eta_{\text{maj}}(\theta) > \eta_{\text{min}}(\theta)$ . For example, along  $x$ , spin down is the minority spin species (cf. Fig. 2). We solve for the zero in the dielectric function corresponding to the spin demon by making the ansatz [27]

$$\omega_d(\mathbf{q}) = v_d \eta_{\text{min}}(\theta) q \quad (7)$$

and requiring  $\omega_d(\mathbf{q})$  to lie in the pseudogap formed by the edges of the spin-resolved particle-hole continua.

We carry out this approach in Sec. VIII in the SM [23], and find that, up to corrections of order  $(q/k_F)^2$ , the spin demon velocity  $v_d$  is determined by

$$4 - \frac{v_d}{v_F} \log \left[ \frac{v_F - v_d}{v_d - v_F} \right] - \frac{v_d \eta_{\text{min}}}{v_F \eta_{\text{maj}}} \log \left[ \frac{v_F \eta_{\text{maj}} - v_d \eta_{\text{min}}}{v_d \eta_{\text{min}} - v_F \eta_{\text{maj}}} \right] = 0. \quad (8)$$

This has no analytical solutions, and we thus solve it numerically.

The above analysis also gives the quality factor, defined as  $Q \equiv \omega_d/\gamma$ , where the damping  $\gamma$  can be obtained by performing a Laurent-Taylor expansion around  $\omega_d$  to find

$$\gamma = \frac{\text{Im}[\epsilon(\mathbf{q}, \omega)]}{\partial_\omega \text{Re}[\epsilon(\mathbf{q}, \omega)]} \Big|_{\omega=\omega_d}. \quad (9)$$

In Fig. 3, we show  $v_d$  and the corresponding quality factor  $Q$  as a function of  $\theta$ . We stress that for quality factors less than unity, the spin demon is no longer a well-defined quasiparticle, which happens for  $\theta_c \geq 23^\circ$  for this set of parameters. Up to this critical angle, the velocity of the spin demon only changes by a factor of 2, while the quality factor falls off by one order of magnitude. The quality factor is not bounded, and increasing the altermagnetic band anisotropy (proportional to  $m_0/m_*$ ) leads to higher quality factors.

*Out-of-phase oscillations and magnetic moment.* To gain more insight in the character of the spin demon, we solve the eigenvalue problem defined by Eq. (1),

$$\begin{pmatrix} \text{Re}[\chi_\uparrow^{(0)}(\omega)]^{-1} - v_q & -v_q \\ -v_q & \text{Re}[\chi_\uparrow^{(0)}(\omega)]^{-1} - v_q \end{pmatrix} \begin{pmatrix} \psi_\uparrow \\ \psi_\downarrow \end{pmatrix} = 0, \quad (10)$$

which has the solution

$$\frac{\psi_{\text{maj}}}{\psi_{\text{min}}} = -\frac{v_q N_0}{1 + v_q N_0} \approx -1 + O(q^2/k_F^2), \quad (11)$$

where  $N_0 = \tilde{m}k_F/(2\pi^2\hbar^2)$  is the spin-independent density of states at the Fermi level. This result thus clearly shows that in the limit of small  $q/k_F$ , the spin demon consists of out-of-phase oscillations of two spin-species—in contrast to the conventional plasmon, which consists of in-phase oscillations

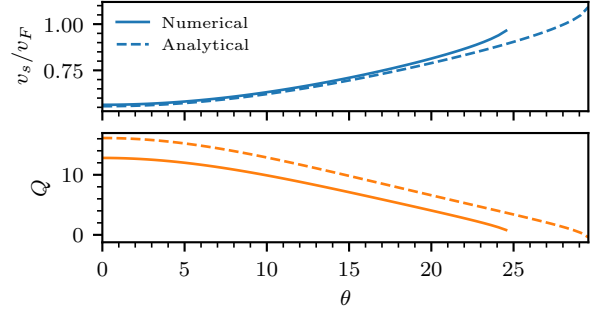


FIG. 3. The spin demon velocity (top) and quality factor (bottom), as a function of angle  $\theta$ . The numerical solutions (solid), are obtained by numerically finding the zeros and corresponding derivatives from the full dielectric function; the analytical solutions (dashed) follow from numerically solving Eq. (8).

[17]. Equation (11) also demonstrates that as  $q/k_F$  approaches zero,  $|\psi_{\text{maj}}| < |\psi_{\text{min}}|$ . We therefore expect that a spin demon carries a magnetic moment, since it is composed of predominantly one spin species.

To show this in more detail, we consider an external magnetic field  $B$  aligned with the Néel vector direction and with a magnitude far below the spin-flop transition. The electrons gain energy  $\sigma g_e \mu_B B$ , with  $g_e \approx 2$  the electron gyromagnetic ratio and  $\mu_B$  the Bohr magneton. We furthermore neglect orbital magnetization effects. We now calculate the magnetic moment, which is defined as

$$\mu_d \equiv -\hbar \frac{\partial \omega_d}{\partial B}. \quad (12)$$

In the limit of  $\eta_{\text{min}}(\theta)/\eta_{\text{maj}}(\theta) \rightarrow 0$  we have

$$\frac{\partial v_d}{\partial B} = v'_d \frac{\partial \Delta}{\partial B} + O(\Delta^2), \quad (13)$$

where  $\Delta \equiv g_e \mu_B B N'_0 / N_0$ ,  $v'_d = 8e^{-4}v_F$  and  $N'_0 = \partial N_0(\epsilon)/\partial \epsilon|_{\epsilon=\epsilon_F}$ . This allows us to obtain the magnetic moment as

$$\mu_d = g_e \mu_B \hbar \frac{N'_0}{N_0} \eta_{\text{min}}(\theta) v'_d q. \quad (14)$$

Importantly, a finite magnetic moment implies that a spin demon can carry angular momentum. In addition, since the minority spin species switches between spin-up and spin-down as the spin demon is rotated through the plane, the magnetic moment has the opposite sign for  $\mathbf{q} \parallel \hat{\mathbf{y}}$ , representing the  $d$ -wave symmetry of the underlying altermagnetic bandstructure.

We show this in more detail in Fig. 4, where we have numerically calculated the magnetic moment of the spin demon as a function of  $\theta$ . For the angles where the spin-up species is the majority species, we obtain a positive magnetic moment,

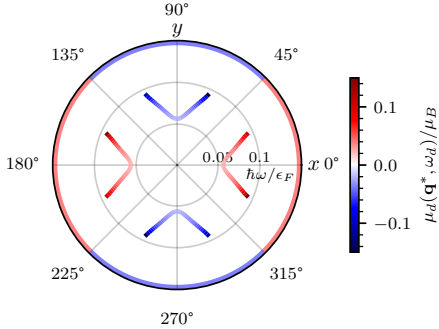


FIG. 4. Numerically obtained spin demon resonance frequency  $\omega$  as a function of  $\mathbf{q}^* = q(\cos \theta, \sin \theta, 0)$ , with  $q = 0.05k_F$ , rotated in the alternage magnetic spin splitting plane with angle  $\theta$ . The color corresponds to the magnetic moment, showing the  $d$ -wave character. Obtained by numerically finding the zeros and evaluating Eq. (12) from the full dielectric function. Along  $x$  and  $y$ , the magnetic moment is approximately  $\pm 0.025\mu_B$ . The colors on the ring indicate the projected spin species.

whereas for the angles where the spin-down species is dominant, we have a negative magnetic moment. The magnetic moment thus captures the  $d$ -wave symmetry of the underlying alternage magnetic bandstructure [Eq. (14)]. For  $q = 0.05k_F$ , we obtain that  $\mu_p \approx 0.025\mu_B$  for  $\mathbf{q} \parallel \hat{\mathbf{x}}$ . The magnetic moment grows to  $0.1\mu_B$  for angles approaching the critical angle—but the quality factor also decreases.

These results show that an applied magnetic field will shift the spin demon frequencies up or down, depending on the orientation of  $\mathbf{q}$ . The shift in the spin demon frequency is however small, approximately  $1.5\mu\text{eV}$  at  $\mathbf{q} = 0.05k_F\hat{\mathbf{x}}$  with a magnetic field of 1 T, whereas the energy of the spin demon is 2.8 meV, resulting in a relative shift of 0.1%. Larger relative shifts might be realized by strain through piezomagnetism [5].

*Two-dimensional.* The spin demon also exists in two-dimensional alternage magnets. The analysis in 2D is similar to in 3D, and we relegate details to Sec. IX in the SM [23]. We choose the same parameters as in 3D.

We show the resulting the imaginary part of the spin-spin response function in Fig. 5, highlighting the same four-fold rotational symmetry. In addition, we show the spin demon velocity and quality factor as a function of the projected spin splitting in 2D. Because the particle-hole continuum is sharply defined in two dimensions, we are able to provide analytical solutions of the spin demon velocity and quality factor as [17]

$$v_d^{2D} = \frac{2}{\sqrt{3}} v_F \eta_{\min}(\theta) q + O(q^2/k_F^2) \quad (15)$$

$$Q^{2D} = \frac{3 \sqrt{4\eta_{\min}^2(\theta) - 3\eta_{\max}^2(\theta)}}{\eta_{\min}(\theta)} + O(q^2/k_F^2), \quad (16)$$

for  $2\eta_{\min}(\theta) > \sqrt{3}\eta_{\max}(\theta)$ , whereas the spin demon ceases to exist if this condition is not met.

We observe that the spin demon in two dimensions is more robust than in 3D, surviving for larger  $\theta$  ( $39.9^\circ$  versus  $\approx 23^\circ$ ).

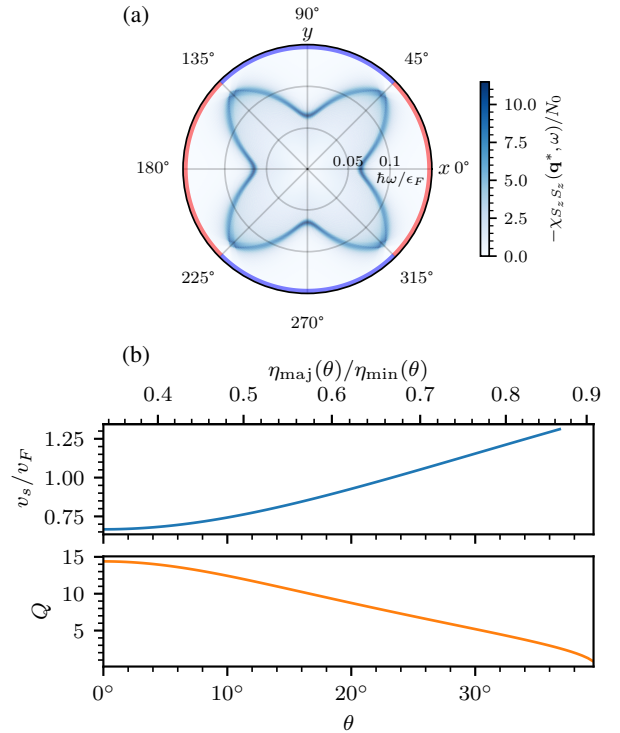


FIG. 5. In two dimensions: (a)  $\text{Im}[\chi_{S_z S_z}(\mathbf{q}^*, \omega)]$ , The angle indicates  $\theta$  and the radial axis the frequency  $\omega$ . (b) The spin demon velocity (top) and quality factor (bottom) as a function of rotation angle  $\theta$ .

Beyond this angle we observe the remnants of the overdamped conventional acoustic plasmon. The quality factors are however comparable in magnitude, especially for angles that align with the alternage magnetic axis. Finally, we comment that in 2D, the spin demon also has a magnetic moment (shown in Sec. IX in the SM [23]), which is comparable in magnitude to the 3D case and displays the same alternage symmetry.

*Conclusion.* We have shown that both three and two dimensional alternage magnetic metals can host out-of-phase oscillations of the two spin densities, realizing a spin demon. The spin demon has a magnetic moment, which changes sign for propagation along different angles through the alternage magnetic plane, inheriting the alternage  $d$ -wave symmetry. We have considered only the RPA, which we expect to provide a fair description, since corrections to the RPA have been shown to mainly enhance the damping of comparable acoustic plasmons in a two-dimensional spin-polarized electron gas [28]. Furthermore, Fermi liquid descriptions of demons have shown no considerable differences compared to the RPA approach [29]. We expect similar conclusions to hold for alternage magnetic spin demons.

In this work, we have considered a  $d$ -wave alternage magnet, where the spin-split Fermi surfaces are elliptical. We have repeated the same analysis for a  $g$ -wave alternage magnet in Sec. X in the SM [23], where we find that the separation of the spin-polarized particle-hole continua is not sufficient for a spin de-

mon to emerge. We therefore conclude that the spin demon is a specific feature of  $d$ -wave altermagnets.

The spin demon could be directly observed by making use of spin-sensitive electron scattering probes, such as spin-polarized electron energy loss spectroscopy (SPEELS) [30] or cross-polarized Raman scattering [31]. These probes directly measure  $\text{Im}[\chi_{S_z S_z}(\mathbf{q}, \omega)]$  (or  $\text{Im}[\chi_{n S_z}(\mathbf{q}, \omega)]$ ), which also contains information of the spin demon; see Sec. III in the SM [23]), and can thus map out Fig. 1 and Fig. 2(a). SPEELS is typically resolution limited in the 10 meV to 100 meV scale [32, 33]. The spin demon exists up to energies of half the Fermi energy  $\epsilon_F$ , as shown in Sec. VI in the SM [23], where the Fermi level of typical  $d$ -wave altermagnets is of the order 500 meV [2]. This would put the spin demon within the resolution range of SPEELS.

Real samples will most likely consist of multiple magnetic domains with different orientations of the Néel vector. We expect that this will not be a difficulty for the detection of the spin demon, since typical domain sizes in altermagnets can be in the micrometer range [34], placing an upper limit on the spin demon wavelength of micrometers. A probe which is spatially localized on this length scale can therefore directly detect spin demons. In addition, recent transport experiments have measured a finite anomalous Hall effect signal, demonstrating that altermagnetic domains are not equally populated [35–37], and thus even a spatially delocalized probe could detect spin demons.

We thank Khalil Zakeri for insightful discussions. This work is in part funded by the Deutsche Forschungsgemeinschaft (DFG, German Research Foundation) – Project No. 504261060 (Emmy Noether Programme) and TRR 173 – 268565370 (project A03 and B13). P. G. acknowledges financial support from the Alexander von Humboldt postdoctoral fellowship.

---

\* pgunnink@uni-mainz.de

- [1] L. Šmejkal, J. Sinova, and T. Jungwirth, Beyond Conventional Ferromagnetism and Antiferromagnetism: A Phase with Non-relativistic Spin and Crystal Rotation Symmetry, *Physical Review X* **12**, 031042 (2022).
- [2] L. Šmejkal, J. Sinova, and T. Jungwirth, Emerging Research Landscape of Altermagnetism, *Physical Review X* **12**, 040501 (2022).
- [3] R. Zarzuela, R. Jaeschke-Ubiergo, O. Gomonay, L. Šmejkal, and J. Sinova, Transport theory and spin-transfer physics in  $d$ -wave altermagnets (2024), arXiv:2412.13763 [cond-mat].
- [4] C.-T. Liao, Y.-C. Wang, Y.-C. Tien, S.-Y. Huang, and D. Qu, Separation of Inverse Altermagnetic Spin-Splitting Effect from Inverse Spin Hall Effect in RuO<sub>2</sub>, *Physical Review Letters* **133**, 056701 (2024).
- [5] T. Aoyama and K. Ohgushi, Piezomagnetic properties in altermagnetic MnTe, *Physical Review Materials* **8**, L041402 (2024).
- [6] K. V. Yershov, V. P. Kravchuk, M. Daghofer, and J. van den Brink, Fluctuation-induced piezomagnetism in local moment altermagnets, *Physical Review B* **110**, 144421 (2024).
- [7] S. Karube, T. Tanaka, D. Sugawara, N. Kadoguchi, M. Kohda, and J. Nitta, Observation of Spin-Splitter Torque in Collinear Antiferromagnetic RuO<sub>2</sub>, *Physical Review Letters* **129**, 137201 (2022).
- [8] M. Naka, S. Hayami, H. Kusunose, Y. Yanagi, Y. Motome, and H. Seo, Spin current generation in organic antiferromagnets, *Nature Communications* **10**, 4305 (2019).
- [9] Z. Liu, M. Ozeki, S. Asai, S. Itoh, and T. Masuda, Chiral Split Magnon in Altermagnetic MnTe, *Physical Review Letters* **133**, 156702 (2024).
- [10] L. Šmejkal, A. Marmodoro, K.-H. Ahn, R. González-Hernández, I. Turek, S. Mankovsky, H. Ebert, S. W. D’Souza, O. Šípr, J. Sinova, and T. Jungwirth, Chiral Magnons in Altermagnetic RuO<sub>2</sub>, *Physical Review Letters* **131**, 256703 (2023).
- [11] D. Pines, Electron interaction in solids, *Canadian Journal of Physics* **34**, 1379 (1956).
- [12] A. A. Husain, E. W. Huang, M. Mitrano, M. S. Rak, S. I. Rubeck, X. Guo, H. Yang, C. Sow, Y. Maeno, B. Uchoa, T. C. Chiang, P. E. Batson, P. W. Phillips, and P. Abbamonte, Pines’ demon observed as a 3D acoustic plasmon in Sr<sub>2</sub>RuO<sub>4</sub>, *Nature* **621**, 66 (2023).
- [13] J. Ruvalds, Are there acoustic plasmons?, *Advances in Physics* **30**, 677 (1981).
- [14] S. Das Sarma and A. Madhukar, Collective modes of spatially separated, two-component, two-dimensional plasma in solids, *Physical Review B* **23**, 805 (1981).
- [15] K. Sadhukhan, A. Politano, and A. Agarwal, Novel Undamped Gapless Plasmon Mode in a Tilted Type-II Dirac Semimetal, *Physical Review Letters* **124**, 046803 (2020).
- [16] A. N. Afanasyev, A. A. Greshnov, and D. Svintsov, Acoustic plasmons in type-I Weyl semimetals, *Physical Review B* **103**, 205201 (2021).
- [17] A. Agarwal, M. Polini, G. Vignale, and M. E. Flatté, Long-lived spin plasmons in a spin-polarized two-dimensional electron gas, *Physical Review B* **90**, 155409 (2014).
- [18] C. M. Varma, Mixed-valence compounds, *Reviews of Modern Physics* **48**, 219 (1976).
- [19] S. K. Sinha and C. M. Varma, Possibility of acoustic plasmons in mixed-valence metals and their interaction with phonons, *Physical Review B* **28**, 1663 (1983).
- [20] J. Ihm, M. L. Cohen, and S. F. Tuan, Demons and superconductivity, *Physical Review B* **23**, 3258 (1981).
- [21] G. Giuliani and G. Vignale, *Quantum Theory of the Electron Liquid* (Cambridge University Press, 2005).
- [22] S. Ahn and S. Das Sarma, Anisotropic fermionic quasiparticles, *Physical Review B* **103**, 045303 (2021).
- [23] See Supplemental Material at [URL will be inserted by publisher] for a detailed calculation of the spin resolved response functions, details on the numerics, analytical solutions for the spin demon dispersion, quality factor and magnetic moment, and the spin demon in two dimensions and in  $g$ -wave altermagnets.
- [24] A. Kamenev, *Field Theory of Non-Equilibrium Systems*, 2nd ed. (Cambridge University Press, 2023).
- [25] S. Kaltenborn and H. C. Schneider, Plasmon dispersions in simple metals and Heusler compounds, *Physical Review B* **88**, 045124 (2013).
- [26] J. Lindhard, On the properties of a gas of charged particles, *Kgl. Danske Videnskab. Selskab Mat.-fys. Medd.* **28**, No. 8 (1954).
- [27] G. E. Santoro and G. F. Giuliani, Acoustic plasmons in a conducting double layer, *Physical Review B* **37**, 937 (1988).
- [28] D. Kreil, R. Hobbiger, J. T. Drachta, and H. M. Böhm, Excitations in a spin-polarized two-dimensional electron gas, *Physical Review B* **92**, 205426 (2015).

- [29] A. N. Afanasiev, Acoustic plasmons and isotropic short-range interaction in two-component electron liquids, *Physical Review B* **106**, 10.1103/physrevb.106.224301 (2022).
- [30] M. Plihal, D. L. Mills, and J. Kirschner, Spin Wave Signature in the Spin Polarized Electron Energy Loss Spectrum of Ultrathin Fe Films: Theory and Experiment, *Physical Review Letters* **82**, 2579 (1999).
- [31] J. Kim, J.-U. Lee, and H. Cheong, Polarized Raman spectroscopy for studying two-dimensional materials, *Journal of Physics: Condensed Matter* **32**, 343001 (2020).
- [32] D. Vasilyev and J. Kirschner, Design and performance of a spin-polarized electron energy loss spectrometer with high momentum resolution, *Review of Scientific Instruments* **87**, 083902 (2016).
- [33] K. Zakeri, J. Wettstein, and C. Sürgers, Generation of spin-polarized hot electrons at topological insulators surfaces by scattering from collective charge excitations, *Communications Physics* **4**, 225 (2021).
- [34] O. J. Amin, A. Dal Din, E. Golias, Y. Niu, A. Zakharov, S. C. Fromage, C. J. B. Fields, S. L. Heywood, R. B. Cousins, F. Maccherozzi, J. Krempaský, J. H. Dil, D. Kriegner, B. Kiraly, R. P. Campion, A. W. Rushforth, K. W. Edmonds, S. S. Dhesi, L. Šmejkal, T. Jungwirth, and P. Wadley, Nanoscale imaging and control of altermagnetism in MnTe, *Nature* **636**, 348 (2024).
- [35] S. G. Jeong, S. Lee, B. Lin, Z. Yang, I. H. Choi, J. Y. Oh, S. Song, S. wook Lee, S. Nair, R. Choudhary, J. Parikh, S. Park, W. S. Choi, J. S. Lee, J. M. LeBeau, T. Low, and B. Jalan, Metallicity and Anomalous Hall Effect in Epitaxially-Strained, Atomically-thin RuO<sub>2</sub> Films (2025), arXiv:2501.11204 [cond-mat].
- [36] M. Leiviskä, J. Rial, A. Bad'ura, R. L. Seeger, I. Kounta, S. Beckert, D. Kriegner, I. Joumard, E. Schmoranzerová, J. Sinova, O. Gomonay, A. Thomas, S. T. B. Goennenwein, H. Reichlová, L. Šmejkal, L. Michez, T. Jungwirth, and V. Baltz, Anisotropy of the anomalous Hall effect in thin films of the altermagnet candidate Mn<sub>5</sub>Si<sub>3</sub>, *Physical Review B* **109**, 224430 (2024).
- [37] H. Reichlova, R. Lopes Seeger, R. González-Hernández, I. Kounta, R. Schlitz, D. Kriegner, P. Ritzinger, M. Lammel, M. Leiviskä, A. Birk Hellenes, K. Olejník, V. Petříček, P. Doležal, L. Horak, E. Schmoranzerova, A. Badura, S. Bertaina, A. Thomas, V. Baltz, L. Michez, J. Sinova, S. T. B. Goennenwein, T. Jungwirth, and L. Šmejkal, Observation of a spontaneous anomalous Hall response in the Mn<sub>5</sub>Si<sub>3</sub> d-wave altermagnet candidate, *Nature Communications* **15**, 4961 (2024).